Application of gel polymer electrolytes based on ionic liquids in lithium-sulfur batteries

M. Baloch, A. Vizintin, R.K. Chellappan, J. Moskon, D. Shanmukaraj, Rémi Dedryvère, T. Rojo, R. Dominko

Application of Gel Polymer Electrolytes Based on Ionic Liquids in Lithium-Sulfur Batteries

Marya Baloch,[a, b, =] Alen Vizintin,[c,=] Rajesh Kumar Chellappan,[d] Joze Moskon,[c] Devaraj Shanmukaraj,[a] Rémi Dedryvère,[d, e] Teofilo Rojo,[a, b] and Robert Dominko[c, e, *]

[a] CIC Energigune, Parque Tecnológico de Álava, CIC 01510 Miñano, Spain

[b] Departamento de Química Inorgánica, Universidad del País Vasco UPV/EHU, 48080 Bilbao, Spain

[c] National Institute of Chemistry, 1000 Ljubljana, Slovenia

[d] IPREM, CNRS, University Pau & Pays Adour, 64053 Pau cedex 9, France

[e] Alistore - European Research Institute, 80039 Amiens cedex, France

=These authors equally contributed to this work.

[z]E-mail: Robert.Dominko@ki.si

Abstract

In this study, a gel polymer electrolyte (GPE) based on polymer ionic liquid (PIL) is used in a solvent-free and in a hybrid electrolyte configuration for Li-S batteries. Results obtained in the solvent-free configuration show a high discharge capacity in the first cycle and excellent coulombic efficiency during cycling. Capacity fading and polarization increase during cycling are explained based on the XPS and EIS measurements. The results of the present study are indicating that the increase of various internal resistance contributions and capacity fading are related with an accumulation of polysulfides in the GPE-PIL layer or/and on the surface of the lithium anode. Within a hybrid battery configuration, the thickness of the GPE-PIL layer is thinner, and the volume where polysulfides can be trapped is smaller. Such a configuration shows better cycling stability. The hybrid configuration outperforms cycling stability of the conventional configuration with a liquid electrolyte. This is explained by increased internal resistance in the convential configuration while the polarization in the first 100 cycles is constant in the hybrid configuration. Additionally, the hybrid configuration exhibits excellent C-rate performance.

Manuscript submitted May 26, 2016; revised manuscript received August 3, 2016. Published xx xx, xxxx.

1. Introduction

Lithium-sulfur (Li-S) batteries possess high theoretical specific capacity at potential of 2.15 V and are expected to reach practical gravimetric energy density up to 600 Wh kg^{-1}.[1–4] Sulfur is an abundant and easy element to handle. However, at room temperature is an insulator and requires to be properly electrochemically wired.

Li-S battery working principles and the problems within system has been well-known for decades.[5–7] During discharge, two well defined plateaus at 2.4 V and 2.15 V, represent equilibrium states between solid-state phase (either elemental sulfur or Li_2S) and polysulfides, respectively.[8] Recent research has been mainly focused on the development of suitable host structures for sulfur *i.e.* porous structured carbons or oxide based materials.[3,9–15] In addition, attention has been drawn towards the development of new binders,[16,17] separators,[18–20] electrolytes[21–23] and lithium protection.[24,25]

Different types of electrolyte solvents (organic, aqueous and ionic liquids), salts, additives and states (liquid, solid or polymer) has been proposed and tested in Li-S batteries. Most of the work has been done with electrolytes based on ether solvents which are stable towards polysulfides and possess high polysulfide solubility. Their major drawback is a severe shuttle effect.[26] Polymer and solid-state electrolytes can suppress the shuttling effect, although the rate capability is poor compared to liquid electrolytes.

Gel polymer electrolytes are the hybrid of conventional and solid polymer electrolytes with an embedded liquid component, *i.e* an electrolyte in a polymer matrix. Due to an immobilized electrolyte, enhanced ionic conductivity is achieved, when compared to solid-state electrolytes.[26] Moving from liquid to polymer electrolyte systems, safety of the battery system enhances due to reduced probability for internal short-circuiting, absence of volatile reaction products and no electrolyte leakage.[26–29] Gel polymer electrolytes is an attractive choice for Li-S batteries[26,30–33] since it can simultaneously act as a binder and electrolyte due to the

presence of polymer material. Currently, polyvinylidene fluoride (PVdF)[16] is the most common used binder in Li-S batteries, processed by dissolving in *N*-methyl-2-pyrrolidone (NMP). Generally electrode processing requires high drying temperatures under vacuum[34] that could lead to sulfur sublimation whereas, drying at lower temperatures leaves a possibility of contamination with remaining NMP solvent.[34] In addition, the morphology of hydrophobic polymers such as PVdF, blocks the pores[35] in the composite electrode, which limits the electrolyte access and thereby affects ionic pathways. Recently the use of alternative binders, such as polyvinyl pyrrolidone (PVP),[36] polytetrafluoroethylene (PTFE),[37] polyethylene oxide (PEO)[37] and water soluble binders such as carbonyl-β-cyclodextrin (C-β-CD), etc.[17,38,39] has been reported in Li-S batteries.

Herein, we present the application of a gel polymer electrolyte,[40] which can act as an electrolyte and binder in Li-S battery. The GPE (poly(DDA)TFSI-PYR_{14}TFSI-LiTFSI) is composed of 58 wt. % polymer ionic liquid: poly (diallyldimethylammonium) bis(trifluoromethanesulfonyl)imide (poly (DDA)TFSI), and 1:9 mol ratio of ionic liquid: *N*-butyl-*N*-methylpyrrolidinium bis(trifluoromethanesulfonyl)imide (PYR_{14}TFSI) with lithium salt: Lithium bis(trifluoromethylsulphonyl)imide (LiTFSI) as shown in the Figure S1.

The gel polymer electrolyte, GPE-PIL, has been used as a self-standing membrane separator in solvent-free battery configuration and as a binder in the composite cathode. Room temperature cycling was obtained using a hybrid configuration of the cell containing a GPE-PIL combined with liquid electrolyte leading to improved cycling properties compared to conventional Li-S cells solely containing the liquid electrolyte. Due to the pronounced binding properties of the GPE, no additional binder was required in the composite cathode. This led to simplified electrode processing by replacement of NMP with acetonitrile or acetone as a solvent for the composite slurry processing.

2. Experimental

Membrane preparation:

GPE membranes were prepared inside an argon-filled glove box. The GPE-PIL solution was cast on the Mylar film support to form a homogeneous film, dried for over 24 h at room temperature under argon atmosphere. The obtained film was peeled off from the support as a self-standing membrane with thickness of ~200 μm (Figure S2).

Cathode composite preparation and cell assembly:

The gel polymer electrolyte was introduced in the composite cathode by two different methods.

a) Impregnation of as-prepared electrode composites with GPE-PIL: Electrodes casted on aluminum current collector were used with 50 wt. % sulfur loading in mesoporous carbon[41] mixed with PVdF (Sigma-Aldrich, 99.98%) and carbon black (Printex XE2) in a mass ratio of 80:10:10 in NMP. The typical sulfur loading on the electrode was slightly above 1 mg per cm^{-2}. Electrodes were impregnated with the GPE-PIL solution and as a prepared self-standing membrane (4.16 cm^2) was placed on top. The composite electrode was left to dry slowly at room temperature (for at least 24 h). Both steps were carried out inside an argon-filled glove box. The configuration of the solvent-free cell assembly is shown in Figure S3. Briefly, lithium foil (Aldrich) was separated from the impregnated cathode by the GPE-PIL membrane, and electrochemical performance of the obtained stack was measured in pouch cells at 55 °C using C/40 rate in a 1.0–3.8 V voltage range. Galvanostatic measurements were done using a Bio-Logic VMP3 galvanostat/potentiostat.

b) Mixing of sulfur/carbon composite with GPE-PIL. The sulfur/carbon composite was prepared by using DMSO solvent technique. 30 wt. % of carbon black (Ketjan black ECP600JD from AkozoNobel) and 70 wt. % of sulfur (Sigma-Aldrich, 99.98%) were mixed in DMSO and stirred overnight at 155 °C in a closed vial. The obtained

mixture was centrifuged for 45 mins at 400 rpm, the acquired product was dried at 60 °C for 24 h under vacuum. This composite mixture (50 wt. %) was wet ball-milled with 50 wt. % of GPE-PIL for 30 mins in acetonitrile. The slurry was casted on carbon-coated aluminum current collector and dried overnight at 50 °C under vacuum. Electrodes were punched out as spherical discs of 16 mm diameter. The typical sulfur loading on the electrode was around 0.7 mg per cm^{-2}. Pouch cell-type batteries were assembled in an argon-filled glove box. Conventional cathode/electrolyte/anode battery configuration has been followed. GPE-PIL-$C_{ECP600JD}$-S were used as cathode and lithium metal foil (Aldrich) as an anode separated by Celgard 2400 separator wetted with 1M LiTFSI in TEGDME:Diox (vol. 1:1) or 1M LiTFSI in DME:Diox (vol. 1:1) electrolyte. The electrochemical performance was measured at room temperature using C/20 rate in a 1.5–3 V voltage range using a Bio-Logic VMP3 galvanostat/potentiostat.

For comparative evaluation of the electrochemical properties with and without the use of GPE-PIL as binders, conventional cathodes with PVdF binder were prepared by mixing 80 wt. % of C-S composite, 10 wt. % of ECP600JD carbon black and 10 wt. % of PVdF in NMP. The slurry was wet ball-milled for 30 min in NMP and casted on carbon-coated aluminum current collector. Electrodes were dried at 55 °C for 24 h prior to use. Conditions for battery assembly and galvanostatic cycling tests of the PVdF-$C_{ECP600JD}$-S cathodes were exactly the same as in the case of GPE-PIL-$C_{ECP600JD}$-S cathodes.

Impedance spectroscopy:

AC impedance responses were measured using Solartron SI 1260 impedance analyzer coupled with PAR EG&G 283 potentiostat/galvanostat applying voltage-controlled sinusoidal signals in the frequency range from 100 kHz to 1 mHz with an amplitude of 10 mV (rms). Intermittent measurements were carried on the cell for every 2.5 hours during galavanostatic cycling.

X-ray Photoelectron Spectroscopy (XPS):

XPS measurements were carried out with a Kratos Axis Ultra spectrometer with monochromatic Al Kα radiation (hv = 1486.6 eV). Battery opening was done in a controlled argon atmosphere. The samples were transferred into vacuum through a glove box directly connected to the XPS spectrometer without exposure to air or moisture. The binding energy scale was calibrated using a C 1s hydrocarbon contamination peak at 285 eV. The electrodes for the XPS analysis were not washed in any organic solvents before the XPS measurements. Other experimental details has been reported elsewhere.[42]

SEM analysis:

SEM images were measured with a field-emission scanning electron microscope (FE SEM) Supra 35 VP (Zeiss, Germany).

3. Results and discussion

3.1 Contributions of the GPE-PIL components to the internal resistance of the cell

In order to get insight in the various contributions of different components and contacts in the studied Li-S battery configurations we have performed an electrochemical impedance spectroscopy (EIS) measurements. Due to the complexities of the system, we show in this work only preliminary results, which will be discussed more in details in the future.

a) Equivalent circuit of a conventional Li-S cell

A proposed equivalent circuit of a conventional Li-S cell comprising a porous composite cathode is presented in Figure 1. It is split to the corresponding contributions of the cathode, anode and separator layer. The contribution of the electrolyte phase in the separator is presented by parallel coupling of resistance $R_b(sep.)$ and capacitance C_ε which stands for the

capacitance associated with the dielectric relaxation in the electrolyte. Since the corresponding time constant $R_b(sep.) \cdot C_\varepsilon$ is typically in the order of 1 ns up to few 10 ns the impedance contribution of the electrolyte in the separator for the practical frequency range of EIS can usually be regarded as an Ohmic resistance $R_b(sep.)$. The same reasoning holds true for the part of electrolyte that is present in the cathode pores – *i.e.* the parallel coupled pairs of elements $r_{\mathrm{pore,i}} \| c_{\varepsilon,i}$ can be regarded as pure Ohmic resistances $r_{\mathrm{pore,i}}$.

The impedance contribution(s) of the Li-anode side vary during cycling (especially in the initial cycles there is regularly observed a decrease in the anode impedance) similarly as observed in Li-ion systems.[43,44]

The contribution(s) of the porous cathode can be essentially presented by a modified type of the transmission line model that was used for the interpretation of electro-chemical properties of multi-particle Li-ion insertion cathodes.[45,46] A Li-S cathode differs from a Li-ion cathode in two major respects. First, the end members of the conversion reaction are solids with low solubility while the intermediate polysulfides formed during the course of the reaction are soluble in the ether-based electrolytes. Second, electrochemical redox reaction of soluble sulfur species proceeds at the accessible surface of electronically conductive matrix while chemical equilibrium tends to be established within the volume of electrolyte by means of reaction between different sulfur species. As a consequence, the concentration gradients of different sulfur species build up during the operation of the Li-S cell and simultaneously an inevitable diffusion of those species is taking place. Although during operation of the Li-S cell the situation in the electrolyte and at surface of conductive matrix is greatly complex compared to the Li-ion cell. The impedance response of the Li-S cell in a quasi-equilibrium state can be in a simplified manner treated similarly to a Li-ion cell with multi-particle porous insertion cathode. When applying a small a.c. voltage signal during impedance measurement of a quasi-equilibrated Li-S cell the variations of concentrations of the present

sulfur species are small and for the present purpose we neglect the effect of these concentration variations on the ion transport in the electrolyte. The cathode composite is assumed to be homogeneous – thus it can be split in the serially connected electrochemically equivalent "layers" as shown in the Figure 1a.

b) High-frequency intercept R_s (conventional liquid electrolytes)

At high frequencies in MHz range some capacitance elements such as C_ε and $c_{\varepsilon,i}$ (Figure 1b) are already "open" – *i.e.* the associated displacement current practically ceases, thus the corresponding coupled resistances of electrolyte in the separator ($R_b(sep.)$) and in pores of cathode composite ($r_{\mathrm{pore,i}}$) appear as a pure resistances and it can be considered as a main contribution for R_s. Most of the other capacitance elements have much larger magnitudes (higher time constants and can be neglected).

At the high-frequency equivalent circuit there are no elements related to Li-anode – thus according to the present interpretation Li-anode does not contribute to R_s. This is strictly valid for "smooth" non-cycled Li-anode (as for example anode in initial state after cell assembly). During cycling surface morphology of metal Li gradually becomes more and more "roughened" and eventually even disintegrated during repeatable Li stripping and platting.[43,47,48] In that way a sort of porous-like Li-anode is formed that can bring contribution to R_s.

Thus we find that the contribution of cathode to R_s is composed of two parts: a) Contribution of porous composite that amounts in the equivalent resistance for the parallel combination of $R_{\mathrm{cath.}}$ and R_{pore}; b) Contribution of interface at the surface of current collector that amounts in the equivalent resistance for the parallel combination of r_0 and $r_{\mathrm{pore},0}$. Therefore, in principle both pairs ($R_{\mathrm{cath.}} \| R_{\mathrm{pore}}$ and $r_0 \| r_{\mathrm{pore},0}$) do contribute partially to R_s. However, in real cells the second pair can be generally neglected, as the resistance of element $r_{\mathrm{pore},0}$ is

very small. In practice, for a cathode to give rise of a significant contribution to R_s its electronic ($R_{\text{cath.}}$) and ionic (R_{pore}) resistances would have to be largely increased at the same time. For Li-S cells with conventional liquid electrolytes this is rather unlikely to be the case during individual discharge/charge – for instance during discharge the precipitation of solid Li_2S can reduce electrode porosity and thereby increase R_{pore}, but in the initial part of the same discharge insulating elemental sulfur is consumed which might even decrease the $R_{\text{cath.}}$. On the contrary, during long term cycling $R_{\text{cath.}}$ might gradually increase due to: i) loosen electronic connectivity of the composite (reduced mechanical integrity due to local volume changes associated with repeatable dissolution/precipitation of solid S_8 and Li_2S phases); ii) possible (chemical/electrochemical) formation of electronically non-conductive films at the surface of conductive matrix and/or carbon black particles; and iii) decreased conductivity of electrolyte in the pores. These effects can result in a slow gradual increase of R_s during cycling. Thus for Li-S cells with conventional liquid electrolytes the regularly observed peculiar periodic variation of R_s during the course of individual cycle is most probably not related to concurrent increase of the $R_{\text{cath.}} \| R_{\text{pore}}$ pair but rather to the increase of $R_b(sep.)$ alone. Although R_{pore} increases in accordance with the increase of specific bulk resistance of electrolyte (ρ_b) it does not contribute to the R_s as it is "shielded" by low resistance $R_{\text{cath.}}$.

Alternatively, during cycling of a Li-S cell the inclusion/incorporation of the non-conductive products of side reactions (for instance Li_2S) within the native anode passive film at the surface of Li metal anode ($R_{film}(\text{Li})$) can produce additional contributions to R_s.

In the measured R_s there are also included other (minor) Ohmic resistances due to different external (resistance of connection wires – leads, cell terminals) and internal cell electronic contributions (contacts between internal current leads and the two current collectors, electronic resistance of Li-anode). All of these contributions are generally small compared to

the $R_b(sep.)$, R_{pore} and r_0 and more importantly do not vary during the cell operation – thus do not contribute to the observed variation of R_{s}.

c) High-frequency intercept R_{s} (GPE-PIL electrolyte)

For cells that include polymeric or gel type of electrolyte there are additional issues related to viscoelastic properties of such medium exposed to the influence of mechanical stresses that are induced when growth of a new solid phase is taking place in the volume of the medium. For example while discharging the solvent-free Li-S cell a newly formed solid Li_2S phase at the surface of carbon matrix pushes away the adjacent volume of the GPE-PIL thus imposing stresses shear in the electrode. Opposite effect can be expected at the end of charge when solid S_8 is formed. During cycling repeatable formation and decomposition of the two solid phases takes place and consequently binder in the composite is subjected to local variations of stress that can result in severely loosen cathode (electronic) connectivity. Accordingly, the $R_{\mathrm{cath.}}$ greatly increases. Moreover, if at the same time the conductivity of electrolyte in the cathode pores is reduced consequently the contribution of $R_{\mathrm{cath.}} \| R_{\mathrm{pore}}$ pair to R_{s} becomes large. Thus we see that in case of the cells where cathode is impregnated with (solvent-free) GPE-PIL the R_{s} is not dependent solely upon the resistance of electrolyte layer between cathode and anode, but cathode contribution can become important.

3.2 Electrochemical performance of the Li-S batteries that include GPE-PIL components

The schematic view of the cross-section of the three battery configurations used in the present study are shown in the Figure 2.

a) Solvent-free configuration

Results of galvanostatic cycling at C/40 rate obtained at 55 °C with the solvent-free configuration show two characteristic plateaus in the first discharge (Figure 3a). That indicates the mechanism of sulfur conversion into polysulfides at the high voltage plateau and precipitation of Li_2S in the low voltage plateau.[8] The specific discharge capacity in the first cycle exceeds 1400 mAh g^{-1}. Similar to the first discharge, the first charge shows distinctive voltage profiles as observed in the conventional Li-S batteries with ether-based electrolytes. The total polarization in the first cycle (voltage hysteresis at approximately half of the obtained discharge/charge capacity ~390 mV) is slightly higher as compared to the conventional Li-S battery cycled at room temperature (~330 mV).[41] The polarization issues become more pronounced in the subsequent cycles where a severe and continuous increase of the galvanostatic hysteresis can be seen (for instance ~900 mV in the fifth cycle, Figure 3a). The noticeable increase in the internal resistance is reflected by significant capacity fading, for *e.g.* only half of the initial capacity was achieved after the first 10 cycles with an average coulombic efficiency of 98.1% (Figure 3b). In the higher cycles, the increase of polarization can contribut to the corrosion of aluminum current collector caused by high potential during charging In order to understand correlation between the increase of the internal resistance of the cell and consequent increase of the polarization, we performed comparative EIS experiments. Prior to taking measurements, the battery was left for 3 h at 55 °C to thermally equilibrate and stabilize impedance responses. We performed the following repeating sequence: partial discharge (charge) at C/40 for 2.5 h, open-circuit voltage relaxation for 25 minutes, and EIS measurement (1 MHz – 10 mHz). The first two cycles obtained with a repeating sequences of intermittent galvanostatic cycling, voltage relaxations and EIS are shown in Figure 3c. Electrochemical behavior in the first cycle was similar to the one obtained with the continuous galvanostatic cycling, while a prominent decrease of capacity was observed in the second cycle. From the impedance spectra shown in Figure S4, the values

285 of resistive intercept R_s have been collected and the extracted values for both cycles are
286 presented in Figure 3d.
287 Figure 3d shows that during the first discharge there was only mild variation of R_s. Almost
288 monotonous increase from 16.0 Ω up to 21.6 Ω was observed. This is essentially different
289 from the observation found in the conventional Li-S cells, where a very pronounced maxima
290 of R_s is correlated with the increase in the viscosity of electrolyte due to increased
291 concentration of medium chain polysulfides.[49] Measurements during the first charge show
292 such an increase (after ~300 mAh g^{-1}), but in contrast to conventional Li-S cells R_s did not
293 decrease at the end of discharge but rather remained constant (~31 Ω). The value of R_s
294 practically doubled during the first cycle. In the initial part of the second discharge, an abrupt
295 increase of R_s was observed that increased even further, to finally reach ~90 Ω. At the end of
296 the second charge, only minor decrease of R_s was observed. As already discussed above we
297 the observed pronounced increase of R_s to such large values is connected to coupled effects of
298 reduced GPE-PIL conductivity (caused by dissolution of polysulfides) that increases both
299 membrane resistance ($R_b(membr.)$) as well as resistance of GPE-PIL in pores (R_{pore}), and
300 reduced cathode electronic connectivity (increased $R_{\mathrm{cath.}}$).
301 We propose that the thick GPE-PIL layer in solvent-free configuration denotes a larger
302 volume of a medium (larger diffusion distance) in which (additionally) the rate of diffusion of
303 polysulfides is reduced in comparison to conventional liquid electrolytes. Thus, the expected
304 periodical variation of R_s during discharge and charge was not seen (Figure 3c-d), instead an
305 increase is observed. During the discharge, for example, the reduction of R_s does not take
306 place since the cathode cannot "pump back" all the polysulfides that have diffused a certain
307 critical distance into the GPE-PIL phase away from the surface of the cathode conductive
308 matrix. During the experiment with partial discharge (charge) steps combined with open-
309 circuit relaxation and EIS measurements, the increase in the polarization was even more

pronounced in comparison to continous galvanostatic cycling. Faster increase of polarization can be correlated to additional time available for the diffusion of polysulfides (due to relaxation periods). Specifically, during the relaxation periods, the cathode does not collect or "pump back" any of the polysulfides from the GPE-PIL (even those that are normally in the vicinity of the cathode during continous cycling). Thus more of the polysulfides travel deep into the interiors of GPE-PIL, where they become inaccessible for electrochemical transformation and may eventually reach the metallic Li-anode for chemical reduction to take place.

XPS analysis

In order to better investigate the precise mechanisms leading to the polarization and impedance increase in the batteries, we carefully analyzed the internal parts of the cells with XPS. Precisely, two analyzed samples are depicted in Figure S3, *i.e. (i)* the lithium negative electrode surface facing the GPE-PIL electrolyte, and *(ii)* the GPE-PIL electrolyte surface facing the lithium electrode (the sulfur composite cathode impregnated by the GPE-PIL cannot be separated from the GPE-PIL membrane).

XPS results obtained for the Li-anode surface are shown in Figure 4. After the first discharge (Figure 4a), the surface of metallic lithium is covered by several recognizable species. Due to spin-orbit coupling, S 2*p* peaks are split into two components (S $2p_{3/2}$ and S $2p_{1/2}$) with ~1.2 eV binding energy difference and a 2/1 intensity ratio. The main peak (S $2p_{3/2}$ at around 169.4 eV) is assigned to $TFSI^-$ anion.[50] Another weak component is observed at slightly lower binding energy (~167.5 eV). This latter component was already observed by XPS in Li-S batteries and was attributed to S(IV) degradation species of the salt, which could be a sulfite species, such as $LiSO_2CF_3$ or $Li_2(F_3C\text{-}SO_2\text{-}N\text{-}SO_2)$,[42] or even Li_2SO_3 already proposed by Aurbach et. al.[24] The most interesting signals of the spectrum are the two components observed at low binding energy, *i.e.* ~162 and ~163.6 eV (blue and red, respectively). The

components are attributed to the terminal and bridging sulfur atoms of Li_2S_n polysulfides, respectively. The presence of polysulfides at the surface of the metallic Li-anode proves the diffusion and/or migration of these species from the sulfur composite cathode towards the Li-anode through the GPE-PIL electrolyte. Their relative intensity ratio shows that short chain polysulfides are observed at the surface (mainly Li_2S_2). However, the intensity of these two peaks is quite weak and dramatically much lower than in the case of a liquid electrolyte.[42] Moreover, no Li_2S component can be observed after the first discharge. Therefore, it can be concluded that the GPE-PIL electrolyte in solvent-free configuration retards the polysulfide diffusion from the sulfur composite cathode to the Li-anode. Substantial modifications are observed after several cycles. Figure 4b shows the S 2*p* spectrum of the Li-anode after the 5th discharge. In this case, the amount of polysulfides is increased (mainly Li_2S_2), and the largest component of the spectrum (~160.5 eV, pink) is now assigned to Li_2S. Therefore, a significant diffusion of polysulfides have occurred during several cycles, leading to a massive reduction of these species into Li_2S at the surface of metallic Li-anode.

This study was complemented by XPS analysis of the GPE-PIL surface facing the Li-anode, as shown in Figure 5. The XPS S 2*p* spectrum of the pristine GPE-PIL membrane (Figure 5a) shows a unique peak attributed to the $TFSI^-$ anion, as expected. After the first discharge (Figure 5b) the spectrum slightly changes, with the appearance of the aforementioned sulfite degradation compound of the salt, as well as a very weak signature of the polysulfide species. This is in good agreement with the observation of a small amount of polysulfides at the surface of the Li-anode at the end of the first discharge, indicating the passage of polysulfides (to a low extent) across the gel polymer electrolyte.

After the first charge (Figure 5c) the spectrum is not much modified with respect to the first discharge. However, after the 5th discharge (Figure 5d) the S 2*p* spectrum is significantly changed. The amount of polysulfides is multiplied by 20 with respect to the first discharge.

This is in good agreement with the observation of a great amount of Li_2S and short chain polysulfides at the surface of the Li-anode and shows that a great number of polysulfides reaches the opposite surface of the gel polymer electrolyte after several cycles. Note that the bridging-to-terminal sulfur intensity ratio is inverted with respect to the Li-anode surface. This means that longer chain polysulfides are observed at the gel polymer electrolyte surface facing the Li-anode. This is in good agreement with the reduction mechanism of polysulfides (and thus the decrease of their chain length) at the surface of the Li-anode, as expected.

All these XPS observations are consistent with the EIS measurements (variation of R_s) as discussed above.

Although at the present stage of the research of the solvent-free configuration we cannot directly claim which of the contributions to the cell's internal resistance is dominantly responsible for the observed rapid increase of polarization during cycling, the present data and analysis offer several interesting observations and findings:

a) The initial cell polarization is slightly larger compared to the case of Li-S battery with conventional liquid electrolyte (at 25 °C), the difference (~60 mV) being of the magnitude that could be explained by the contribution of the resistance associated with Li^+ ion conduction process in the GPE-PIL components.

b) Pronounced increase of R_s during cycling is indicating that both ionic (R_{pore}) and electronic (R_{cath}) resistances of the cathode have increased, suggesting that internal stresses in the composite might have loosen cathode (electronic) connectivity. Alternatively, formation of Li_2S on Li-anode surface could bring about (or partly contribute) to the observed severe increase of R_s.

c) The GPE-PIL layer does not prevent diffusion of polysulfides but merely hinders it (to diffuse over ~400 μm length during intermittent cycling we estimate that the time needed is ~70 h).

b) Hybrid configuration

In order to minimize the "buffer effect" of the GPE-PIL electrolyte where polysulfides can be trapped and thus becoming unavailable for the main electrochemical transformation, different approach has been studied. One of the possibilities is embedding of the agglomerates of C-S composite in a gel polymer electrolyte without using any additional binder or additional carbon additive. With this approach, 35–60 wt. % of sulfur content has been achieved within the C-S composite. Composites with 10 and 25 wt. % of GPE-PIL showed polysulfides shuttling in early cycles while cycling with 50 wt. % of GPE-PIL exhibits very stable cycling, as shown in Figure 6. To evaluate the performance of composites containing GPE-PIL, a battery in the conventional configuration using PVdF as a binder within the composite electrode has been cycled for comparison. Figure 6 compares three cells, two with gel polymer electrolyte based on PIL using different liquid electrolyte and the third one with PVdF binder. In the formation cycles, about a 20% lower capacity was obtained in the case of PVdF binder using liquid electrolyte (1M LiTFSI TEGDME:Diox), which could be correlated to the hydrophobic nature of PVdF whereby the region of the electrode composite covered with the PVdF are substantially less accessible to Li^+ ions from the electrolyte phase. Surprisingly, batteries with GPE-PIL binder using the same liquid electrolyte (1M LiTFSI TEGDME:Diox) show very similar coulombic efficiency (in average 94%), while the battery with 1M LiTFSI DME:Diox electrolyte shows much higher coulombic efficiency (in average 99.2%). Moreover, working with a low amount of electrolyte has an impact on the cycle life. As can be seen in Figure 6, the capacity of the cell with the PVdF binder exhibited increasing degradation (evident after ~50^{th} cycle) while in contrast the cell with the gel polymer electrolyte showed moderate, practically constant degradation of the capacity until 100 cycles. This observation indicates that the present novel approach in which the binder (PVdF) was

410 replaced with GPE-PIL-based gel demonstrates beneficial properties with enhanced stability
411 of the Li-S electrochemical system.
412 The results are preliminary and after optimization one can expect composites with similar
413 behavior containing a much lower quantity of GPE-PIL. In contrast, this work points out the
414 requirement for optimal thickness, where GPE-PIL presumably serves as a barrier for keeping
415 polysulfides close to the surface of the carbon host matrix. By the present interpretation the
416 role of the "wetted" GPE-PIL is then to prevent the fast diffusion of polysulfides out from the
417 cathode and enable their effective conversion in the discharge or the charge process.
418 However, such pre-treatment allows using a lower amount of liquid electrolyte (GPE-PIL is,
419 in fact, a gel polymer electrolyte). Only one layer of Celgard 2400 separator was used in the
420 battery assembly. Taking the calculated porosity 63 vol. % of porosity of the composite
421 cathode, the amount of electrolyte within the cathode and the separator is between 2–3 μL per
422 1 mg of sulfur. This amount of electrolyte used in our experiment approaches the
423 requirements of achieving a high energy density of the Li-S battery system[4,13]. In this work,
424 we use only one potential gel polymer electrolyte; however, some other types of gel polymer
425 electrolytes based on the polymer ionic liquids are available for any potential improvements.
426 The morphological changes in the cross-section of the electrode after 100 cycles were
427 checked by using SEM. Figure 7a shows the morphology of the composite cathode containing
428 $C_{Ecp600JD}$-S composite covered with 50 wt. % of the GPE-PIL before cycling. The
429 morphological changes after 100 cycles are minor, proving the good stability of the electrodes
430 comprising GPE-PIL-based gel type coating (Figure 7b).
431 Additional information about the cell performance using different components can be
432 obtained by a direct comparison of the galvanostatic curves in different cycles. Figure 8
433 shows the 1^{st}, 10^{th}, 50^{th} and 100^{th} cycles for batteries with gel polymer electrolyte in the
434 composite cathode in combination with two different electrolytes and for the battery with

PVdF binder. The voltage value of the high voltage plateau in the cell with 1M LiTFSI TEGDME: Diox electrolyte (Figure 8a) is approximately 100 mV higher compared to the cell with 1M LiTFSI DME:Diox electrolyte (Figure 8b). The low voltage plateau is relatively flat in both cases, not showing any increase in the polarization during cycling. The discharge curves obtained from the battery with PVdF binder show a pronounced increase of polarization during cycling, particularly at the transition from the high to low voltage plateau, which was observed as a distinctive saddle-like appearing local minima in a voltage profile.

The related increase in polarization is due to oversaturation of the electrolyte with polysulfides, and this gradually increases upon cycling. The reasons for the saturation of the electrolyte with polysulfides can be manifold. Among all the possibilities, the most probable is the saturation of the electrolyte with polysulfides due to continuous polysulfide diffusion out from the composite cathode; additionally, we can expect some electrolyte degradation on the fresh surface of Li-anode formed during the stripping and plating of lithium. In addition to increased polarization, the battery with PVdF binder suffered distinct polysulfide shuttle (Figure 8c).

Kinetic issues shown in the solvent-free configuration compromise the power capability of the battery with the GPE-PIL. However, it is expected that the quantity of the GPE-PIL as well as the quantity of added liquid electrolyte ("wetting condition") in the cell plays very important role in the Li-S battery kinetics. Figure 9a shows rate capability of the battery with 50 wt. % of GPE-PIL in the composite cathode at different current densities corresponding to C/20 to 1C (1.67 mA mg^{-1}) and back to C/20. The capacity drop between C/20 and C/2 corresponds to one third of the initial capacity value, and it is recovered at the slower C-rates. Severe capacity drop occurs as the C-rate is increased up to 1C, as the capacity of the lower plateau cannot be utilized anymore in the voltage window used (1.5–3 V). Figure 9b shows the galvanostatic curves of the rate capability, with the formation cycle at C/50 and going from

C/20 to 1C and back to C/20. Two well defined plateaus are expressed till C/5 rate. At C/2 an increase in polarization is observed, and at 1C a disappearance of the low voltage plateaus. Going back to lower C-rates, the polarization decrease and the low voltage plateau is well defined.

4. Conclusions

Solvent-free configuration of the Li-S battery where the GPE-PIL serves as an electrolyte and as separator offers a system in which the solubility of polysulfides occurs in the ionic liquid nested in the polymer matrix. This battery delivers high initial capacity when operated at elevated temperatures (at 55 °C), and is accompanied with an effect of delayed diffusion of polysulfides through the thick GPE-PIL layer to reach Li-anode. XPS results show that the amount of sulfur species on the lithium surface is very low after the first discharge, while Li_2S and polysulfides can be detected on the lithium surface after several cycles. This was confirmed with EIS, where we observed that the series resistance (R_s) and thus the related bulk resistivity of the GPE-PIL did not show usual periodic increase/decrease behavior during cycling but rather delayed response where the initial mild increase gradually developed in severe rise during 2^{nd} cycle and further remained at that high value. Both these techniques are indicating that larger amounts of polysulfides are inevitably lost in the volume of GPE-PIL of the solvent-free Li-S battery. We cannot conclude if this is the only reason for the increase of polarization at the present stage of the research. More systematic work where increase of interphase resistance on the lithium surface and disintegration of the cathode composite need to be done in the future to understand function of PIL within the Li-S batteries. Furthermore, impact of polysulfide dissolution into GPE-PIL phase will be studied by performing measurements on symmetrical cells and Li-S battery cells.

In the hybrid cell configuration, we prepared the cathodes by embedding the agglomerates of the sulfur/carbon composite in the GPE-PIL electrolyte "coating" without using any additional binder or carbon additive. The long-term cycling stability of electrodes containing the GPE-PIL is improved compared to electrodes using PVdF as a binder. The GPE-PIL layer on the surface of the sulfur/carbon agglomerates in combination with liquid electrolyte probably serves as a buffer where polysulfides are dissolved but, due to slow diffusion in the gel type electrolyte, they are presumably retained within the vicinity of the composite cathode. The hybrid cell configuration offers a system with improved electrochemical stability, where the key role of the GPE-PIL "coating" at the present stage is not understood enough, thus the future efforts will be directed in the study of (chemical, morphological, and transport) properties of the layer at the surface of C/S particles.

Acknowledgements

This research has received funding from the Slovenian Research Agency (J2-5469) and the European Union Seventh Framework Programme under grant agreement No. 314515 (EUROLIS).

Figure captions:

Figure 1: a) Schematic representation of a Li-S battery cell comprising a Li metal anode, a separator soaked with liquid electrolyte and a porous (conductive matrix-sulfur) composite cathode. b) Proposed Equivalent Circuit of a Li-S battery that comprises anode, separator, and a porous (conductive matrix-sulfur) composite cathode. The contribution(s) of the porous cathode can be essentially presented by a modified type of the transmission line model that was used for the interpretation of electro-chemical properties of multi-particle Li-ion insertion cathodes.[45,46] c) Proposed simple High-Frequency (~MHz) Equivalent Circuit. For the meaning and role of the main resistive and capacitive elements see the text.

Figure 2: The schematic view of the cross-section of the a) the solvent-free, b) hybrid and c) conventional configuration.

Figure 3: Tested battery configuration: C/S cathode impregnated with GPE-PIL pressed to a GPE-PIL membrane (thickness of 390 μm) in direct contact with metallic lithium: a) galvanostatic C/40 curves of the 1st, 5th, 15th and 30th cycle measured at 55 °C b) cycling stability c) two cycles of galvanostatic cycling at C/40 rate with relaxation periods after $\Delta x = 0.06$ and d) values of corresponding bulk conductivity R_s extracted from impedance spectra measured at the end of each relaxation period.

Figure 4: XPS S 2*p* spectra of the lithium electrode obtained after a) 1st discharge and b) 5th discharge in solvent-free configurations.

Figure 5: XPS S 2*p* spectra of the GPE-PIL surface facing the Li-anode in solvent-free configurations: a) pristine, b) after 1st discharge, c) after 1st charge and d) after 5th discharge.

Figure 6: Discharge capacity (left y-axis) and coulombic efficiency (right y-axis) for Li-S batteries with GPE-PIL-$C_{Ecp600JD}$-S composite using 1M LiTFSI in TEGDME:Diox electrolyte, GPE-PIL-$C_{Ecp600JD}$-S composite using 1M LiTFSI in DME:Diox electrolyte and PVdF-$C_{Ecp600JD}$-S composite using 1M LiTFSI in TEGDME:Diox. Batteries were cycled with a current density corresponding to C/20 rate between 1.5 and 3 V at RT (25 °C).

Figure 7: SEM micrographs of the GPE-PIL-$C_{Ecp600JD}$-S: a) before cycling and b) after 100 cycles.

Figure 8: Galvanostatic curves in the 1st, 10th, 50th and 100th cycle measured using C/20 rate at RT (25 °C) for the cell configurations: a) GPE-PIL-$C_{Ecp600JD}$-S composite with 1M LiTFSI in TEGDME:Diox using Celgard 2400 separator; b) GPE-PIL-$C_{Ecp600JD}$-S composite with 1M LiTFSI in DME:Diox using Celgard 2400 separator and c) PVdF-$C_{Ecp600JD}$-S composite with 1M LiTFSI in TEGDME:Diox using Celgard 2400 separator.

Figure 9: a) Rate capability of Li-S battery using GPE-PIL-$C_{Ecp600JD}$-S composite, 1M LiTFSI in TEGDME:Diox and Celgard 2400 separator at various discharge and charge rates from C/20 to 1C and back to C/20 obtained at RT (25°C) and b) corresponding galvanostatic curves (solid curves corresponds to applied current densities during increase of the C-rate and dashed curves correspond to decrease of the C-rate).

References

1. P. G. Bruce, S. A. Freunberger, L. J. Hardwick, and J.-M. Tarascon, *Nat. Mater.*, **11**, 19 (2011).

2. B. Dunn, H. Kamath, and J.-M. Tarascon, *Science*, **334**, 928 (2011).

3. A. Rosenman, E. Markevich, G. Salitra, D. Aurbach, A. Garsuch, and F. F. Chesneau, *Adv. Energy Mater.*, **5**, 1500212 (2015).

4. M. Hagen, D. Hanselmann, K. Ahlbrecht, R. Maça, D. Gerber, and J. Tübke, *Adv. Energy Mater.*, **5**, 1401986 (2015).

5. R. D. Rauh, F. S. Shuker, J. M. Marston, and S. B. Brummer, *J. Inorg. Nucl. Chem.*, **39**, 1761 (1977).

6. R. D. Rauh, K. M. Abraham, G. F. Pearson, J. K. Surprenant, and S. B. Brummer, *J. Electrochem. Soc.*, **126**, 523 (1979).

7. Y. V. Mikhaylik and J. R. Akridge, *J. Electrochem. Soc.*, **151**, A1969 (2004).

8. R. Dominko, M. U. M. Patel, V. Lapornik, A. Vizintin, M. Koželj, N. N. Tušar, I. Arčon, L. Stievano, and G. Aquilanti, *J. Phys. Chem. C*, **119**, 19001 (2015).

9. X. Ji, K. T. Lee, and L. F. Nazar, *Nat. Mater.*, **8**, 500 (2009).

10. Y.-X. X. Yin, S. Xin, Y.-G. G. Guo, and L.-J. J. Wan, *Angew. Chem. Int. Ed.*, **52**, 13186 (2013).

11. S. Evers and L. F. Nazar, *Acc. Chem. Res.*, **46**, 1135 (2013).

12. R. Demir-Cakan, M. Morcrette, F. Nouar, C. Davoisne, T. Devic, D. Gonbeau, R. Dominko, C. Serre, G. Férey, and J. M. Tarascon, *J. Am. Chem. Soc.*, **133**, 16154 (2011).

13. M. A. Pope and I. A. Aksay, *Adv. Energy Mater.*, **5**, 1500124 (2015).

14. S. Evers, T. Yim, and L. F. Nazar, *J. Phys. Chem. C*, **116**, 19653 (2012).

15. Y. Yang, G. Zheng, and Y. Cui, *Chem. Soc. Rev.*, **42**, 3018 (2013).

16. S. Urbonaite, T. Poux, and P. Novák, *Adv. Energy Mater.*, **5**, 1500118 (2015).

17. J. Wang, Z. Yao, C. W. Monroe, J. Yang, and Y. Nuli, *Adv. Funct. Mater.*, **23**, 1194 (2013).

18. Y.-S. Su and A. Manthiram, *Chem. Commun.*, **48**, 8817 (2012).

19. A. Vizintin, M. U. M. Patel, B. Genorio, and R. Dominko, *ChemElectroChem*, **1**, 1040 (2014).

20. J.-Q. Huang, T.-Z. Zhuang, Q. Zhang, H.-J. Peng, C.-M. Chen, and F. Wei, *ACS Nano*, **9**, 3002 (2015).

581 21. J. Scheers, S. Fantini, and P. Johansson, *J. Power Sources*, **255**, 204 (2014).

582 22. S. S. Zhang, *J. Power Sources*, **231**, 153 (2013).

583 23. R. Demir-Cakan, M. Morcrette, Gangulibabu, A. Guéguen, R. Dedryvère, and J.-M.
584 Tarascon, *Energy Environ. Sci.*, **6**, 176 (2013).

585 24. D. Aurbach, E. Pollak, R. Elazari, G. Salitra, C. S. Kelley, and J. Affinito, *J. Electrochem.*
586 *Soc.*, **156**, A694 (2009).

587 25. Z. Lin, Z. Liu, W. Fu, N. J. Dudney, and C. Liang, *Adv. Funct. Mater.*, **23**, 1064 (2013).

588 26. S. Zhang, K. Ueno, K. Dokko, and M. Watanabe, *Adv. Energy Mater.*, **5**, 1500117 (2015).

589 27. M. Armand, *Solid State Ionics*, **69**, 309 (1994).

590 28. P. G. Bruce and C. A. Vincent, *J. Chem. Soc. Faraday Trans.*, **89**, 3187 (1993).

591 29. D. Baril, C. Michot, and M. Armand, *Solid State Ionics*, **94**, 35 (1997).

592 30. J. Jin, Z. Wen, X. Liang, Y. Cui, and X. Wu, *Solid State Ionics*, **225**, 604 (2012).

593 31. K. Jeddi, M. Ghaznavi, and P. Chen, *J. Mater. Chem. A*, **1**, 2769 (2013).

594 32. S. S. Zhang and D. T. Tran, *J. Mater. Chem. A*, **2**, 7383 (2014).

595 33. J. Wang, L. Liu, Z. Ling, J. Yang, C. Wan, and C. Jiang, *Electrochim. Acta*, **48**, 1861
596 (2003).

597 34. H. Schneider, A. Garsuch, A. Panchenko, O. Gronwald, N. Janssen, and P. Novák, *J.*
598 *Power Sources*, **205**, 420 (2012).

599 35. M. J. Lacey, F. Jeschull, K. Edström, and D. Brandell, *J. Phys. Chem. C*, **118**, 25890
600 (2014).

601 36. Z. W. Seh, Q. Zhang, W. Li, G. Zheng, H. Yao, and Y. Cui, *Chem. Sci.*, **4**, 3673 (2013).

602 37. S. Urbonaite and P. Novák, *J. Power Sources*, **249**, 497 (2014).

603 38. M. J. Lacey, F. Jeschull, K. Edström, and D. Brandell, *J. Power Sources*, **264**, 8 (2014).

604 39. Q. Wang, W. Wang, Y. Huang, F. Wang, H. Zhang, Z. Yu, A. Wang, and K. Yuan, *J.*
605 *Electrochem. Soc.*, **158**, A775 (2011).

606 40. G. B. Appetecchi, G.-T. Kim, M. Montanino, M. Carewska, R. Marcilla, D. Mecerreyes,
607 and I. De Meatza, *J. Power Sources*, **195**, 3668 (2010).

608 41. F. Schipper, A. Vizintin, J. Ren, R. Dominko, and T.-P. Fellinger, *ChemSusChem*, **8**, 3077
609 (2015).

610 42. A. Vizintin, M. Lozinšek, R. K. Chellappan, D. Foix, A. Krajnc, G. Mali, G. Drazic, B.
611 Genorio, R. Dedryvère, and R. Dominko, *Chem. Mater.*, **27**, 7070 (2015).

612 43. J.-J. Woo, V. A. Maroni, G. Liu, J. T. Vaughey, D. J. Gosztola, K. Amine, and Z. Zhang,
613 *J. Electrochem. Soc.*, **161**, A827 (2014).

614 44. G. Bieker, M. Winter, and P. Bieker, *Phys. Chem. Chem. Phys.*, **17**, 8670 (2015).

615 45. M. Gaberscek, J. Moskon, B. Erjavec, R. Dominko, and J. Jamnik, *Electrochem. Solid-*
616 *State Lett.*, **11**, A170 (2008).

617 46. J.-M. Atebamba, J. Moskon, S. Pejovnik, and M. Gaberscek, *J. Electrochem. Soc.*, **157**,
618 A1218 (2010).

619 47. C. M. López, J. T. Vaughey, and D. W. Dees, *J. Electrochem. Soc.*, **156**, A726 (2009).

620 48. C. M. López, J. T. Vaughey, and D. W. Dees, *J. Electrochem. Soc.*, **159**, A873 (2012).

621 49. S. Waluś, C. Barchasz, R. Bouchet, J.-C. Leprêtre, J.-F. Colin, J.-F. Martin, E. Elkaïm, C.
622 Baehtz, and F. Alloin, *Adv. Energy Mater.*, **5**, 1500165 (2015).

623 50. R. Dedryvère, S. Leroy, H. Martinez, F. Blanchard, D. Lemordant, and D. Gonbeau, *J.*
624 *Phys. Chem. B*, **110**, 12986 (2006).

625

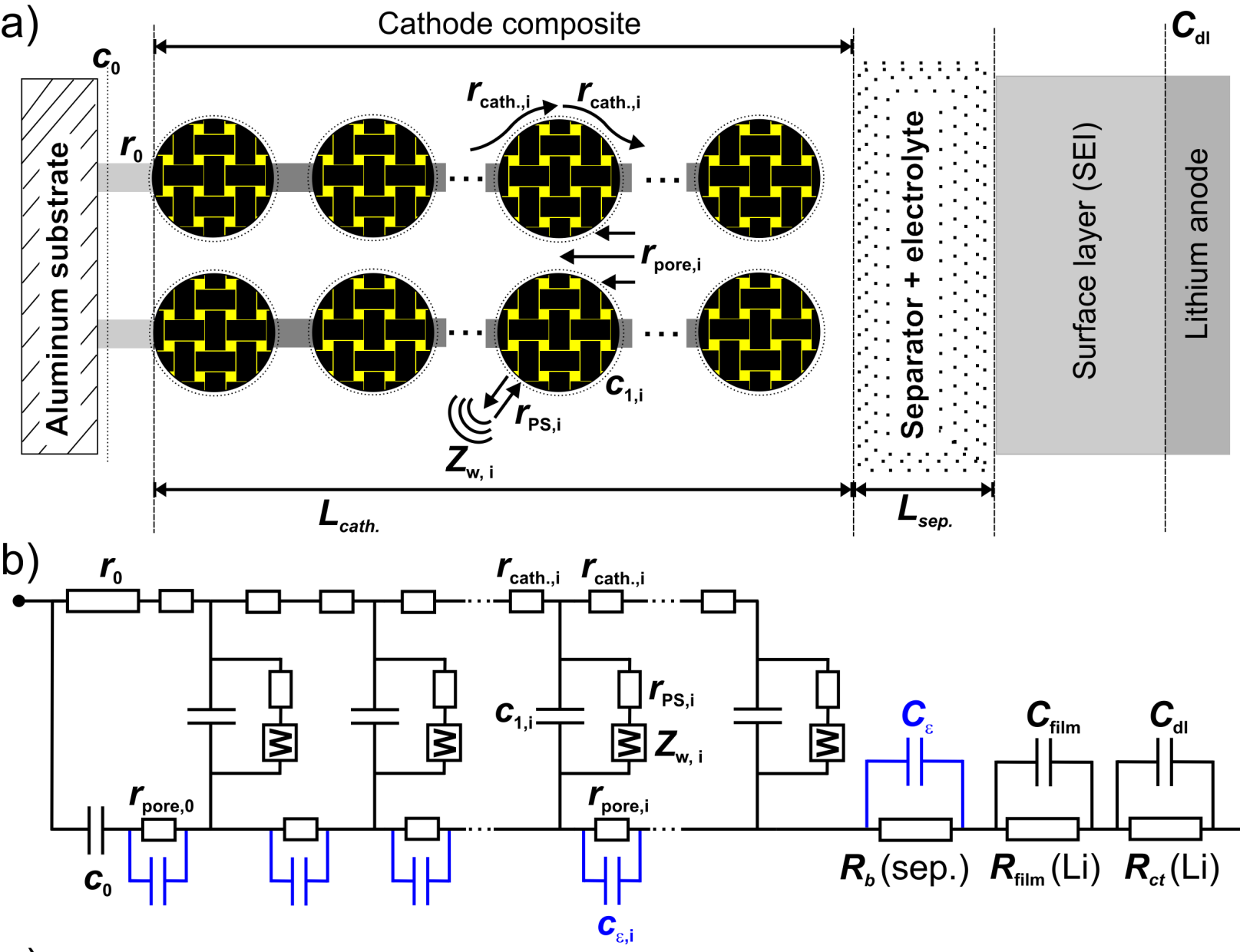
a)
Cathode composite
c_0
r_0
Aluminum substrate
$r_{cath.,i}$
$r_{cath.,i}$
$r_{pore,i}$
$c_{1,i}$
$r_{PS,i}$
$Z_{w,\,i}$
$L_{cath.}$
Separator + electrolyte
$L_{sep.}$
Surface layer (SEI)
Lithium anode
c_{dl}
b)
r_0
$r_{cath.,i}$
$r_{cath.,i}$
$r_{PS,i}$
$c_{1,i}$
$Z_{w,\,i}$
$r_{pore,0}$
$r_{pore,i}$
c_0
$c_{\varepsilon,i}$
c_ε
C_{film}
C_{dl}
R_b (sep.)
R_{film} (Li)
R_{ct} (Li)
c)
r_0
$r_{cath.,0}$
$R_{cath.}$
$r_{pore,0}$
R_{pore}
R_b (sep.)
High-Frequency (MHz)
Equivalent Circuit

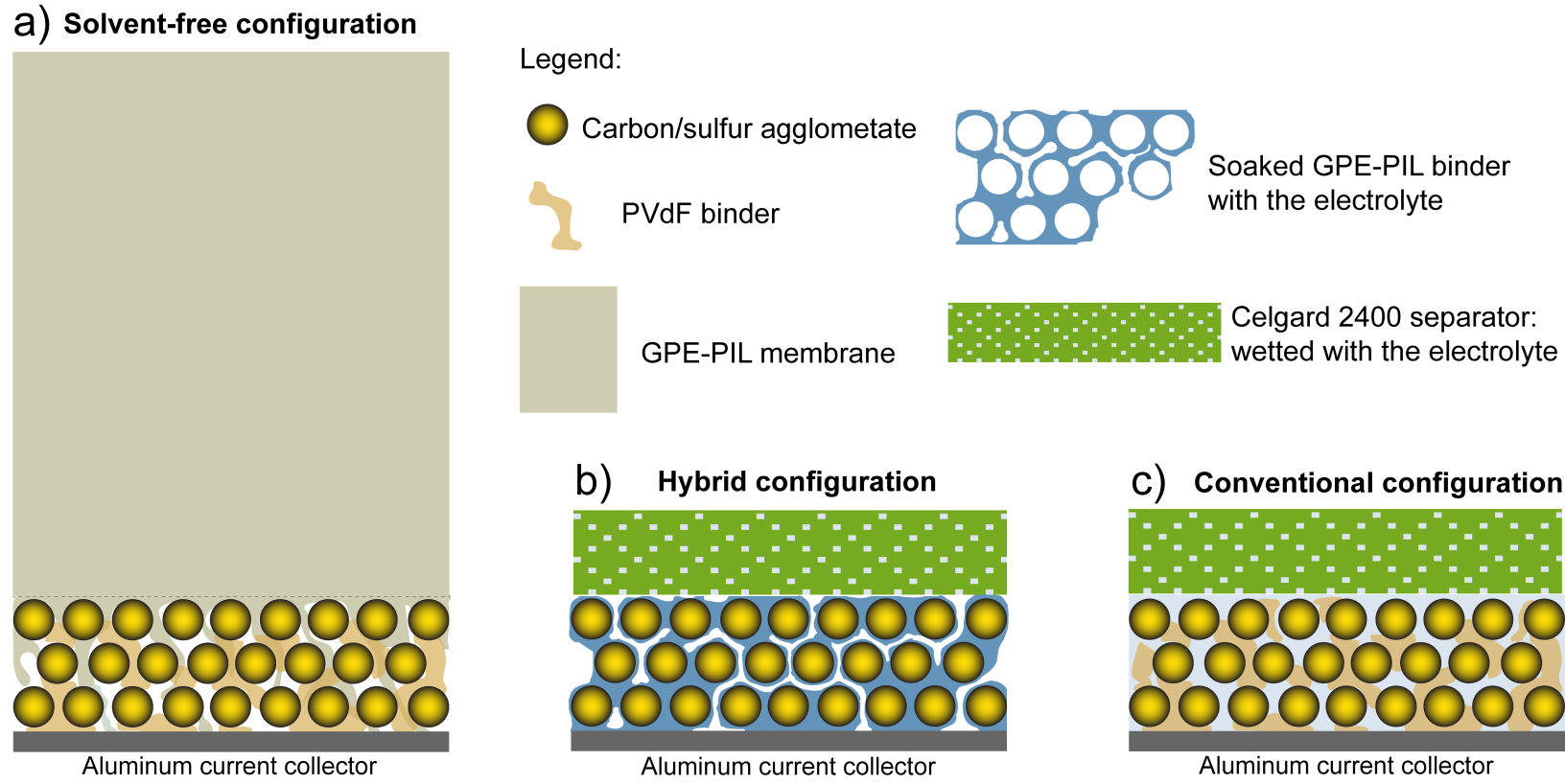
a) Solvent-free configuration
Legend:
Carbon/sulfur agglometate
PVdF binder
GPE-PIL membrane
Soaked GPE-PIL binder with the electrolyte
Celgard 2400 separator: wetted with the electrolyte
b) Hybrid configuration
c) Conventional configuration
Aluminum current collector
Aluminum current collector
Aluminum current collector

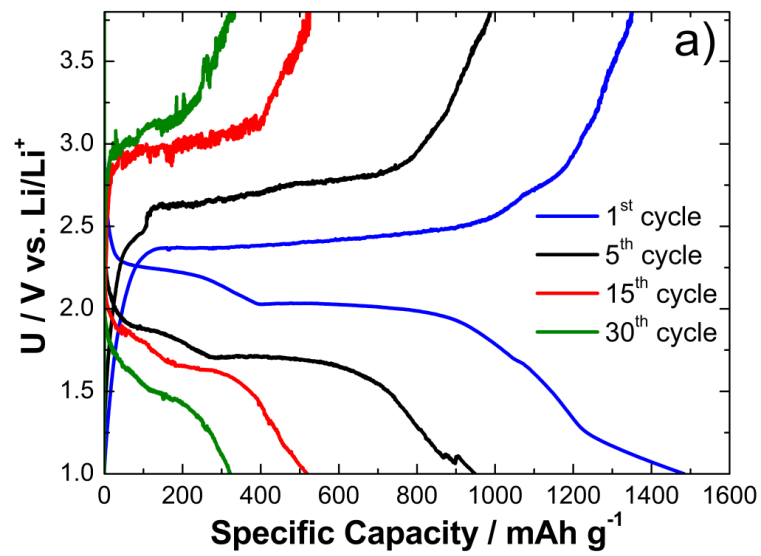
a)
U / V vs. Li/Li+
Specific Capacity / mAh g-1
1st cycle
5th cycle
15th cycle
30th cycle

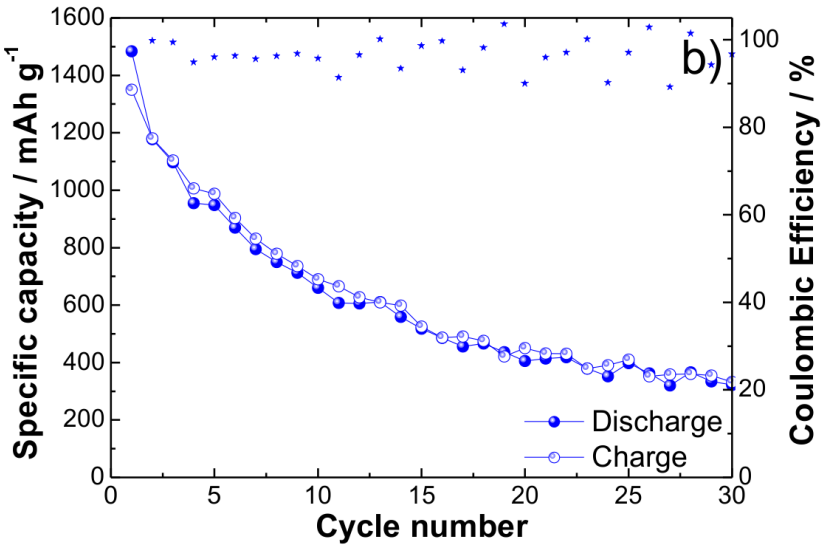
b)
Specific capacity / mAh g-1
Coulombic Efficiency / %
Cycle number
Discharge
Charge

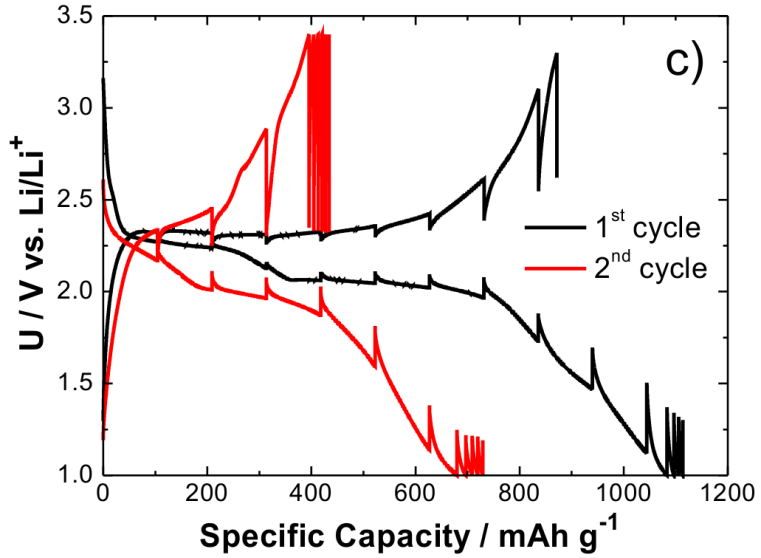
c)
U / V vs. Li/Li+
Specific Capacity / mAh g-1
1st cycle
2nd cycle

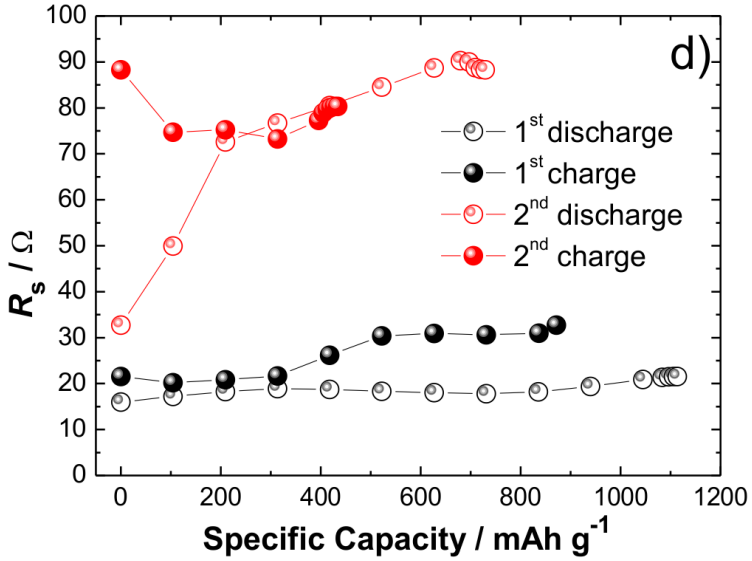
d)
Rs / Ω
Specific Capacity / mAh g-1
1st discharge
1st charge
2nd discharge
2nd charge

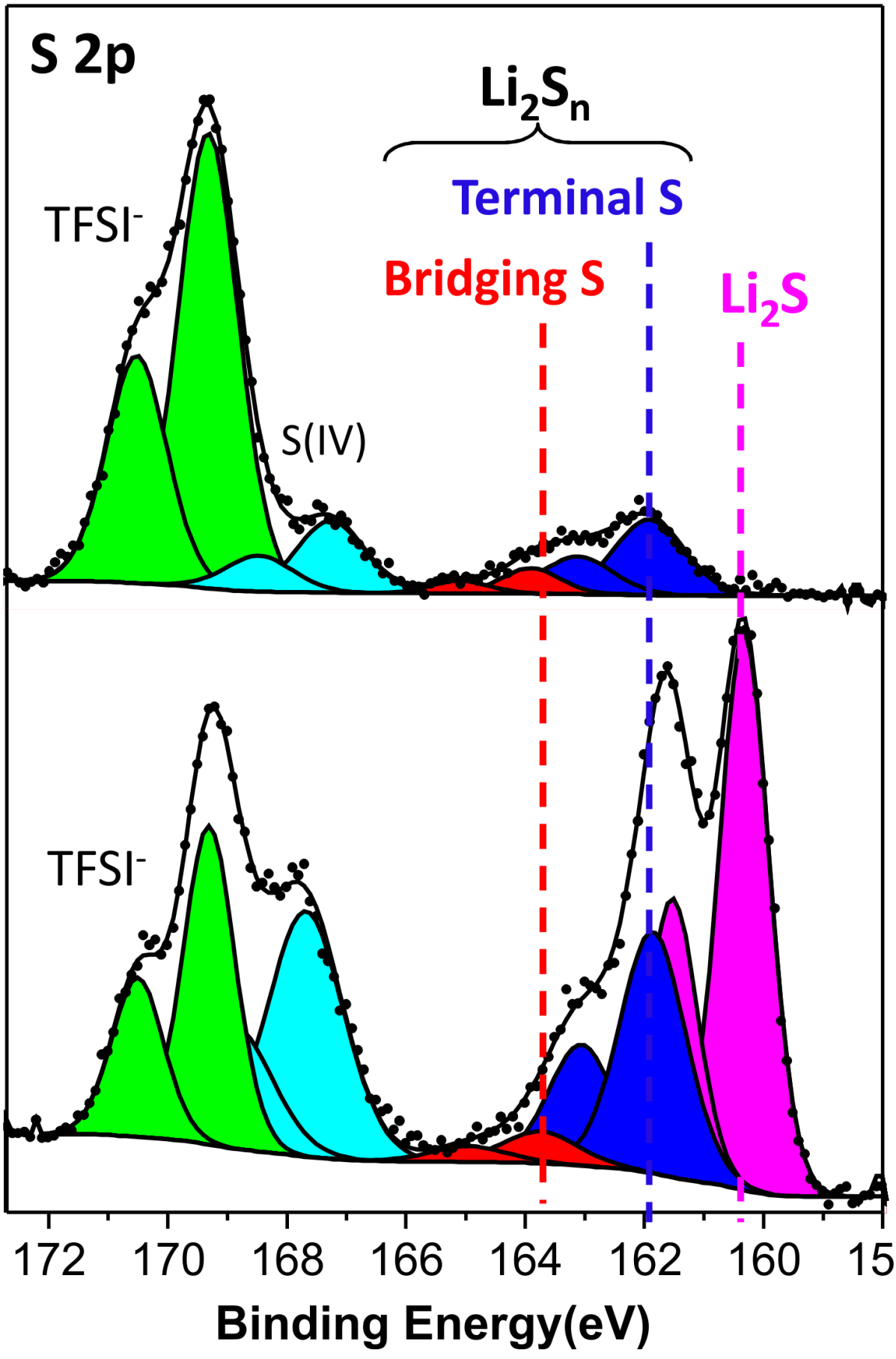

a) 1st discharge

b) 5th discharge

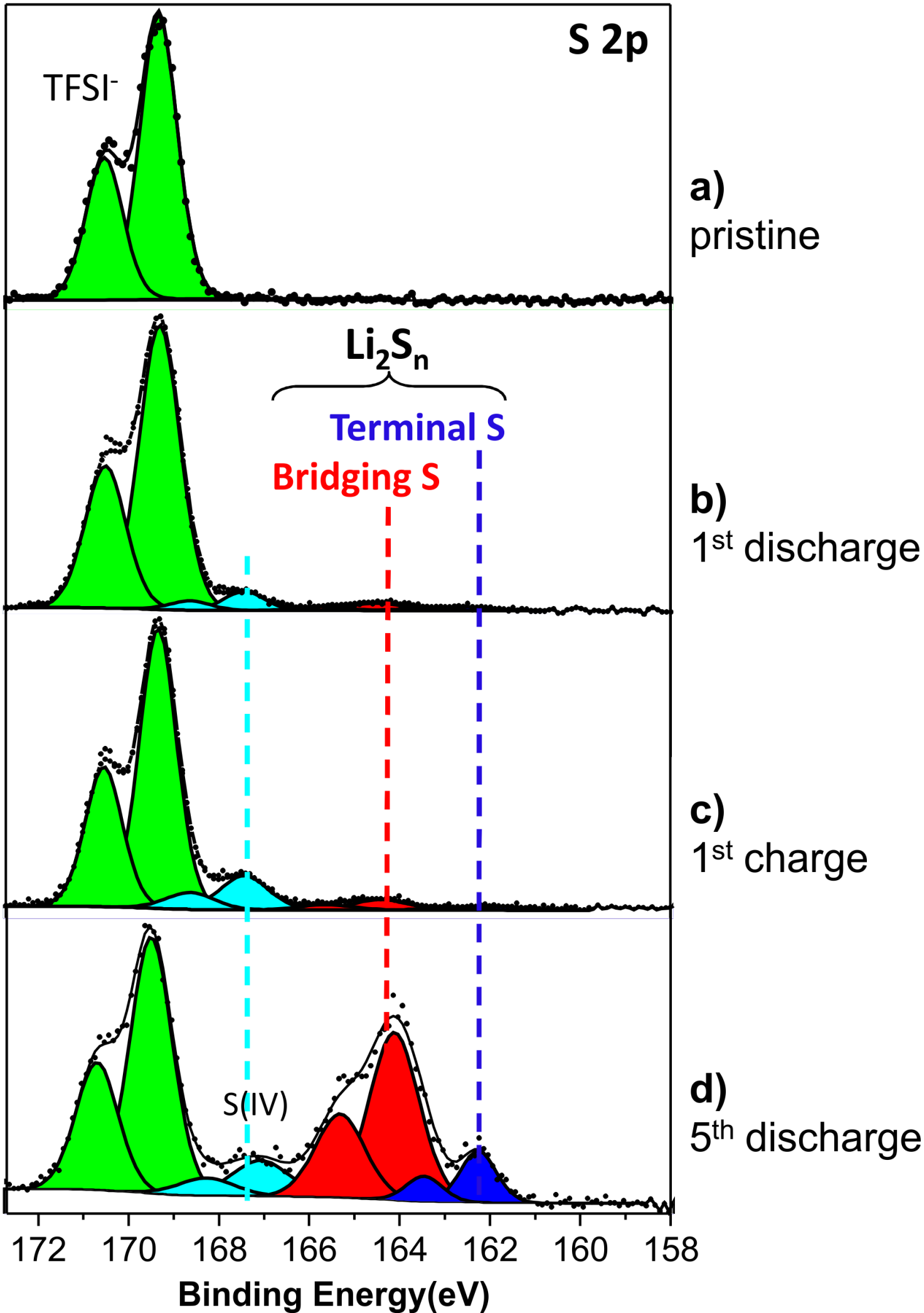
S 2p
TFSI-
a)
pristine
Li2Sn
Terminal S
Bridging S
b)
1st discharge
c)
1st charge
S(IV)
d)
5th discharge
172
170
168
166
164
162
160
158
Binding Energy(eV)

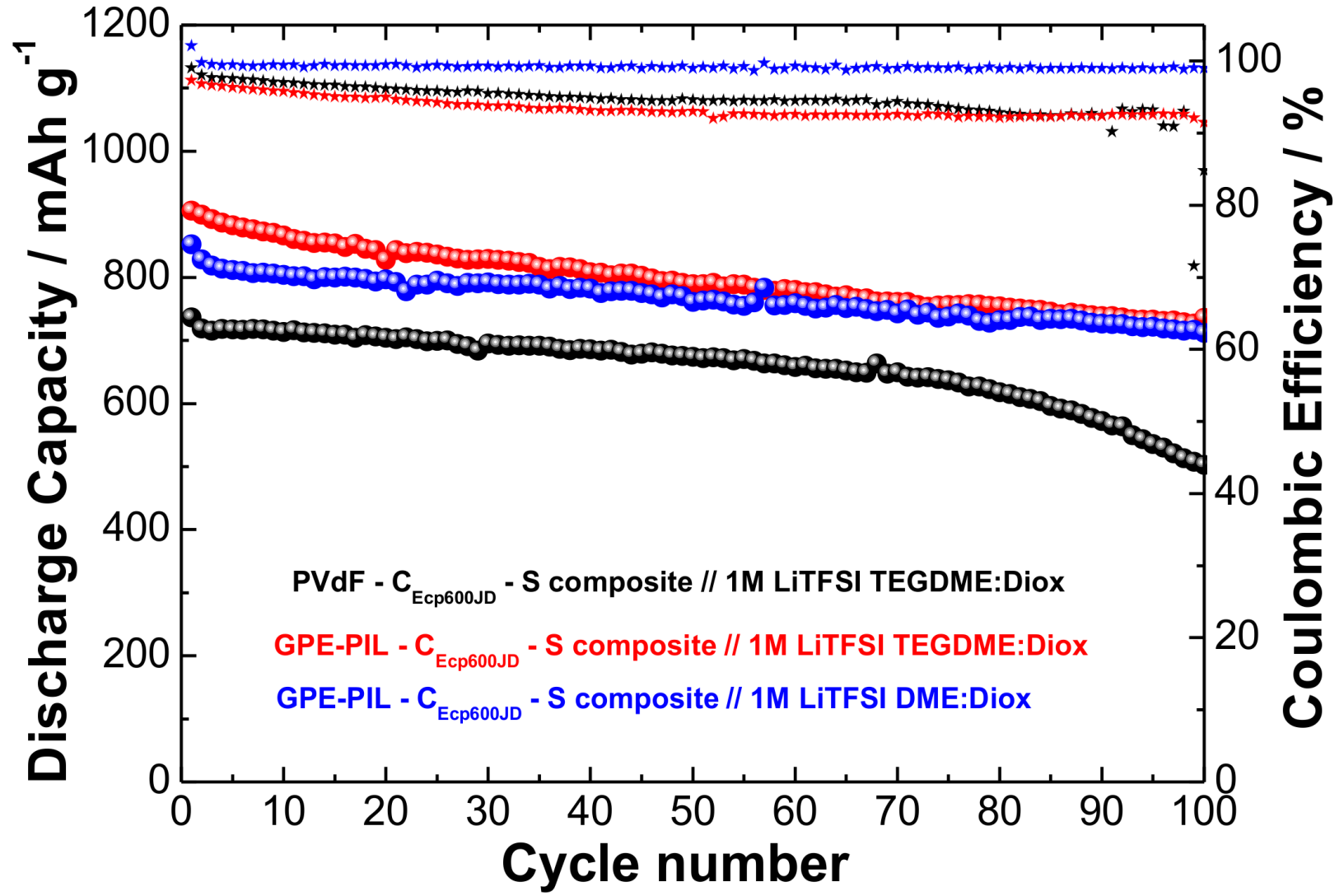
Discharge Capacity / mAh g-1
Coulombic Efficiency / %
Cycle number
0
200
400
600
800
1000
1200
0
20
40
60
80
100
0
10
20
30
40
50
60
70
80
90
100
PVdF - CEcp600JD - S composite // 1M LiTFSI TEGDME:Diox
GPE-PIL - CEcp600JD - S composite // 1M LiTFSI TEGDME:Diox
GPE-PIL - CEcp600JD - S composite // 1M LiTFSI DME:Diox

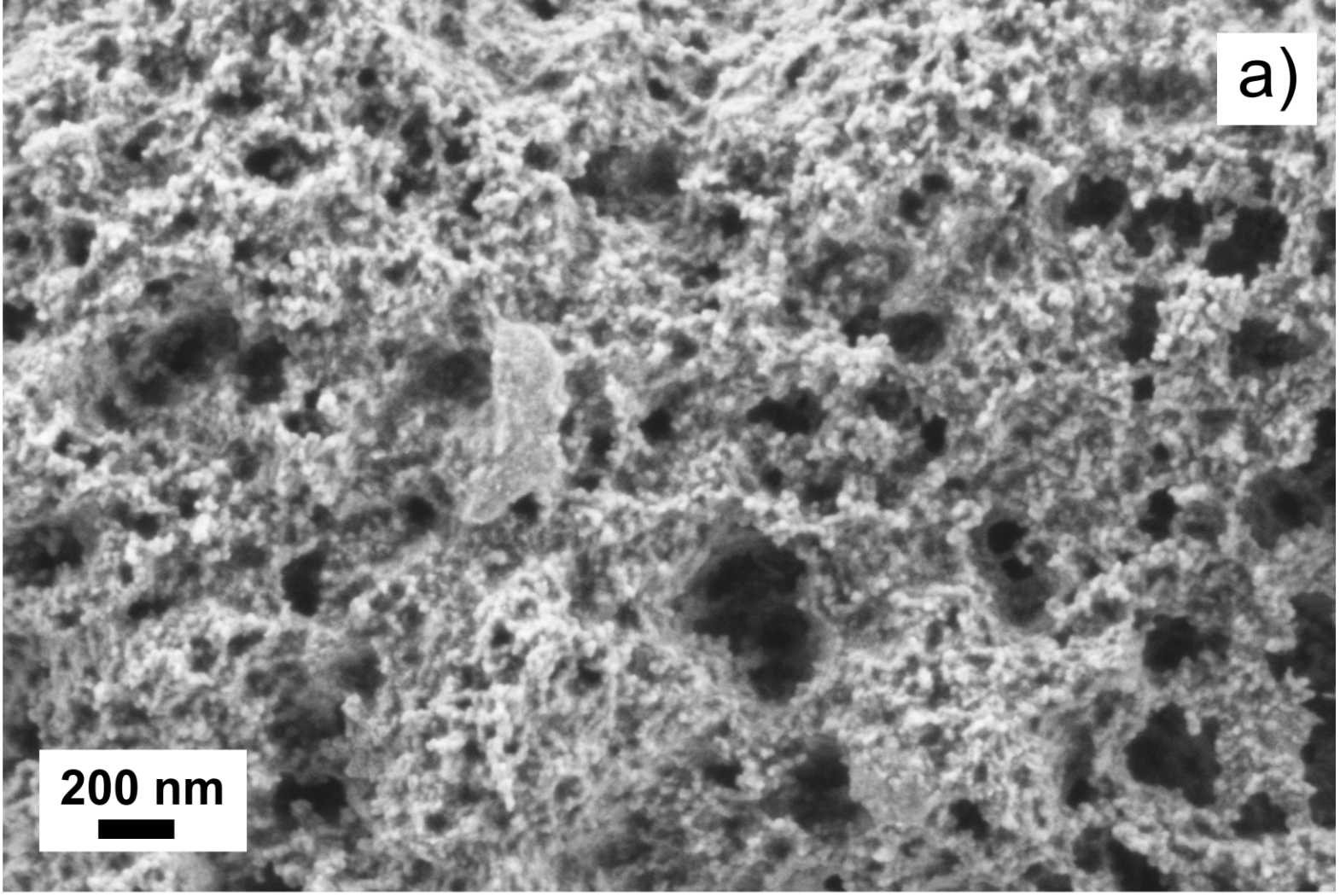
a)
200 nm

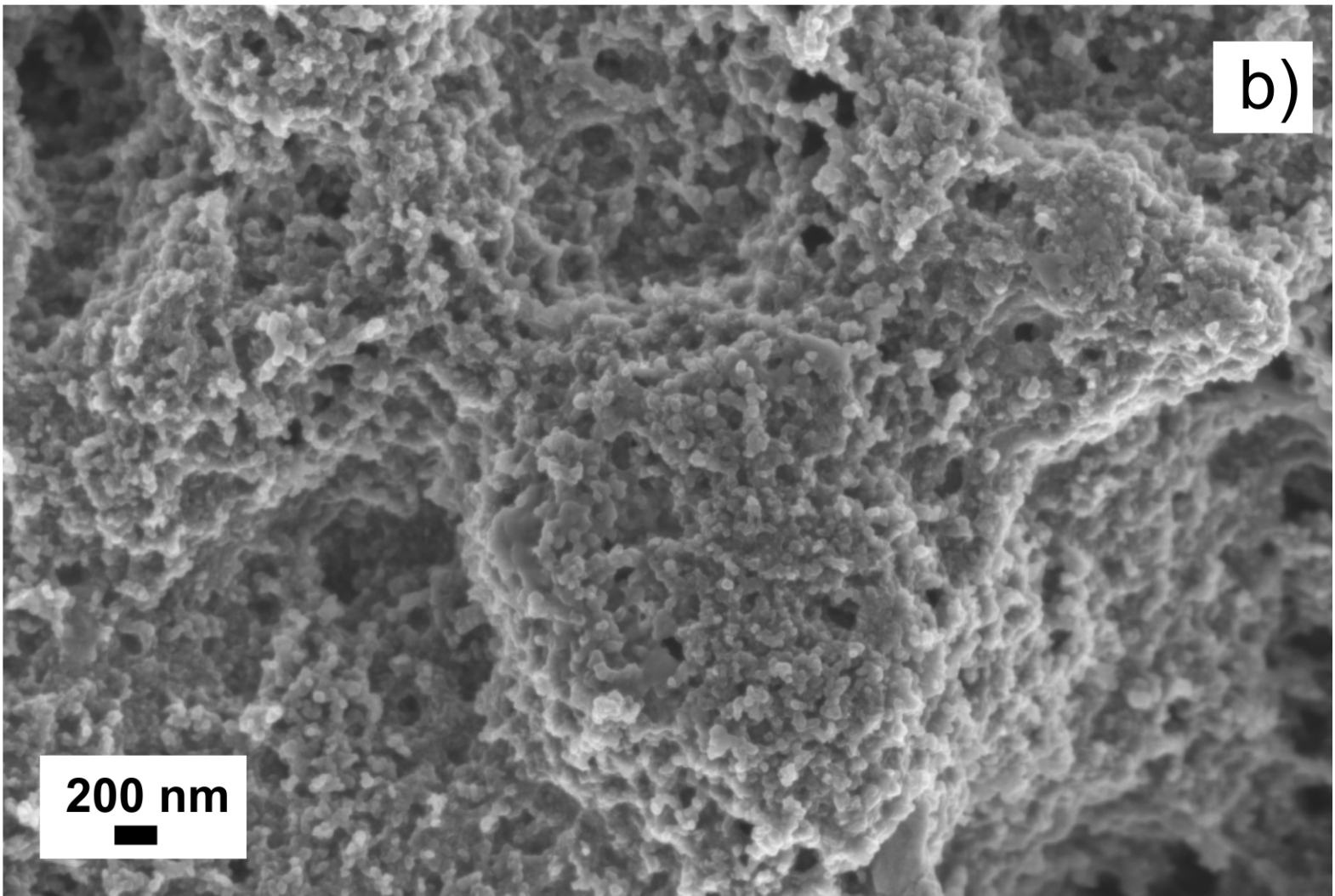
b)
200 nm

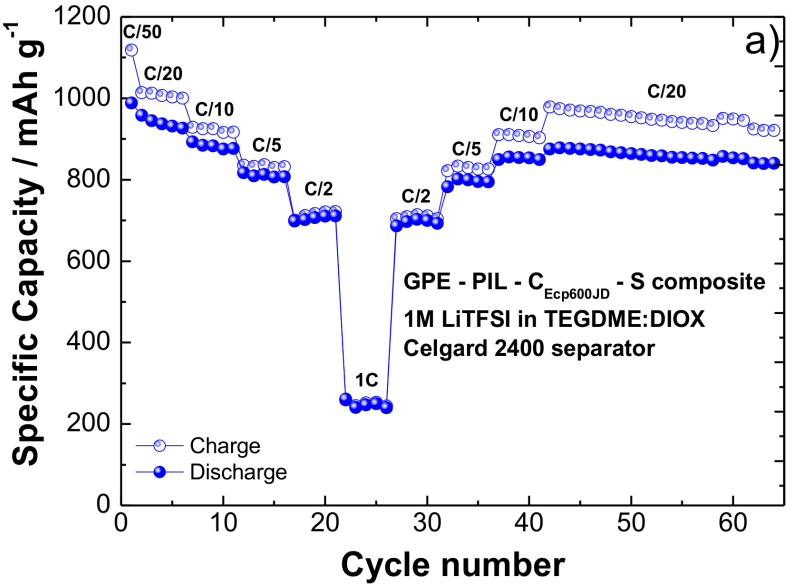
a)
Specific Capacity / mAh g-1
Cycle number
C/50
C/20
C/10
C/5
C/2
1C
C/2
C/5
C/10
C/20
GPE - PIL - CEcp600JD - S composite
1M LiTFSI in TEGDME:DIOX
Celgard 2400 separator
Charge
Discharge

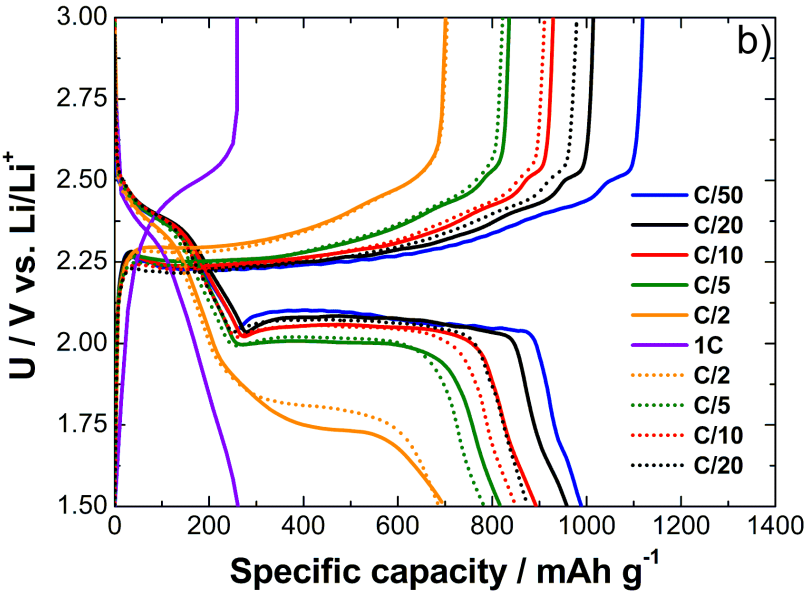
b)
U / V vs. Li/Li+
Specific capacity / mAh g-1
C/50
C/20
C/10
C/5
C/2
1C
C/2
C/5
C/10
C/20

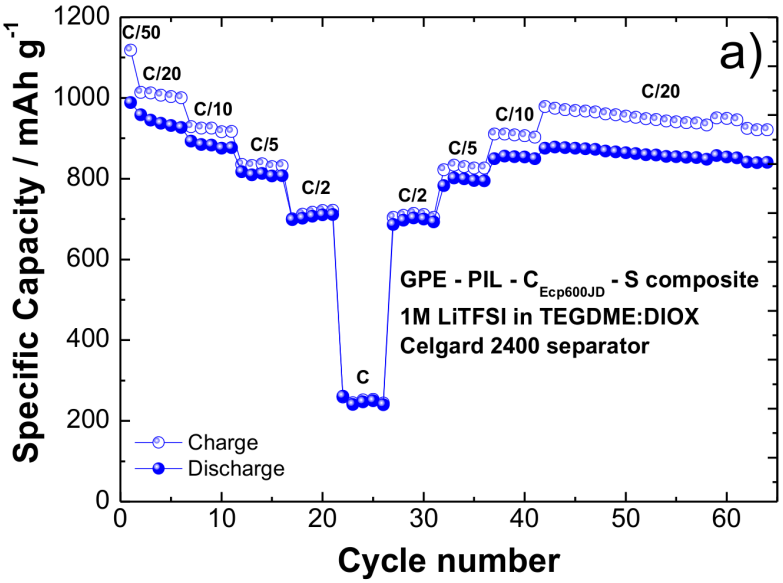
a)
Specific Capacity / mAh g-1
Cycle number
C/50
C/20
C/10
C/5
C/2
C
C/2
C/5
C/10
C/20
GPE - PIL - CEcp600JD - S composite
1M LiTFSI in TEGDME:DIOX
Celgard 2400 separator
Charge
Discharge

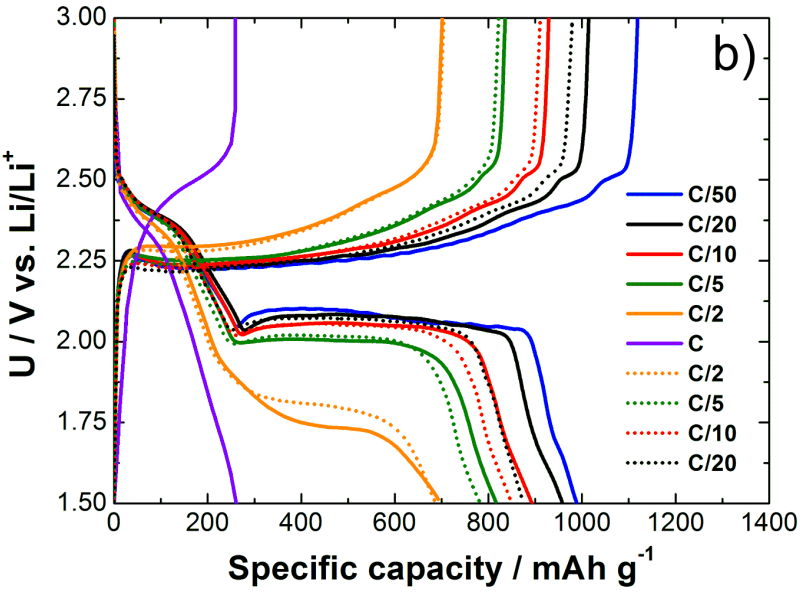
b)
U / V vs. Li/Li+
Specific capacity / mAh g-1
C/50
C/20
C/10
C/5
C/2
C
C/2
C/5
C/10
C/20